Closed-Form Error Propagation on $SE_n(3)$ Group for Invariant EKF With Applications to VINS

Xinghan Li, *Graduate Student Member, IEEE*, Haodong Jiang, Xingyu Chen, He Kong, and Junfeng Wu

***Abstract*—Pose estimation is important for robotic perception, path planning, etc. Robot poses can be modeled on matrix Lie groups and are usually estimated via filter-based methods. In this letter, we establish the closed-form formula for the error propagation for the Invariant extended Kalman filter (IEKF) in the presence of random noises and apply it to vision-aided inertial navigation. Moreover, we use the theoretic results to add the compensation parts for IEKF. We evaluate our algorithms via numerical simulations and experiments on the OPENVINS platform. Both simulations and the experiments performed on the public EuRoC MAV datasets demonstrate that our algorithm in particular parameters settings outperforms some state-of-art filter-based methods such as the quaternion-based EKF, first estimates Jacobian EKF, etc. The techniques of choice on the parameters are worth further investigating.**

***Index Terms*—Invariant extended Kalman filter, localization, visual-inertial SLAM.**

I. Introduction

THE pose estimation problem is highly nonlinear and draws significant research interest. Despite many existing works based on advanced optimization algorithms [1]–[3], the extended Kalman filter (EKF) is recognized as the most widely used method with remarkable merits in terms of computational efficiency and real-time response [4]–[6]. The EKF features linearization of the state-space model about the current state estimate, and inaccurate estimates would degrade the convergence [7] and consistency [8], [9] of the EKF.

Recently, the development of invariant observer design harnesses symmetries (invariance of a dynamical system to some group actions) of nonlinear systems for improved estimation performance [10], [11]. In Barrau and Bonnabel's recent works [12], [13], they analyzed the convergence of the Invariant extended Kalman filtering (IEKF) for noise-free systems, investigating the log-linear property of the invariant error propagation, and revealing the optimality of IEKF. They also proposed error propagation formulas in noisy system via approximating the matrix commutator operation. Later in [14], [15], Martin et al. and Yulin et al. proposed the invariant error propagation in the discrete-time form on $SE_2(3)$ (a matrix Lie group to be discussed in Section II) via the approximation to the *Baker–Campbell–Hausdorff* formula.

This letter studies the invariant error on the special Euclidean group and propagation of the logarithm of the invariant error in the Lie algebra. To the best of our knowledge, this is the first work that presents the closed-form formula of the invariant error propagation in noisy systems without any approximation. Our main contributions are as follows:

i). We establish the closed-form formula of the invariant error propagation for noisy systems without any approximation on the Lie algebra of $SE_n(3)$ and customize the results on $SE_2(3)$. These results provide a theoretical basis to analyze the uncertainty propagation. In addition, we elucidate that the only term that makes this stochastic system nonlinear in the Euclidean Space is the noise term.

ii). We demonstrate the usefulness of the closed-form formula in analyzing and modeling uncertainty propagation in the Inertial Measurement Unit (IMU). First, in the presence of small invariant errors or small IMU bias, we reveal that the exact error propagation can be approximated by a linear stochastic system, which is consistent with the result in [16] by linearization. Moreover, we propose an approximate but simple method of computing the error covariance matrix for propagation through the introduction of an additional random variable imitating the invariant error to compensate the Jacobian term.

iii). We customize the right invariant error result on the $SE_2(3)$ group to IMU and design two filtering algorithms (with/without Jacobian compensation for the calculation of error covariance matrix) for state estimation of a mobile robot with the IMU in a realtime vision-aided inertial navigation system (VINS). We show that two filtering algorithms improve consistency via the observability analysis in [9]. The experimental results illustrate that the proposed filters perform better than state-of-the-art filter-based methods.

We organize the letter as follows. Section II revisits the selected preliminary of the Lie group. Section III establishes the closed-form expression of the invariant error propagation on the extension of the special Euclidean group. Section IV applies the results to IMU navigation models and presents filter design in the VINS. Section V reports the simulation and experiment results. Section VI concludes and envisions future

Manuscript received 24 February 2022; accepted 9 July 2022. Date of publication 28 July 2022; date of current version 9 August 2022. This letter was recommended for publication by Associate Editor J. Civera and Editor K. Khosoussi upon evaluation of the reviewers' comments. This work was supported by the Shenzhen Science and Technology Program under Grant ZDSYS20211021111415025. *(Corresponding author: Xinghan Li.)*

Xinghan Li is with the College of Control Science and Engineering, and the State Key Laboratory of Industrial Control Technology, Zhejiang University, Hangzhou 310027, China (e-mail: xinghanli0207@gmail.com).

Haodong Jiang, Xingyu Chen, and Junfeng Wu are with the School of Data Science, The Chinese University of Hong Kong, Shenzhen 518172, China (e-mail: 221049033@link.cuhk.edu.cn; 987591109@qq.com; junfengwu@cuhk.edu.cn).

He Kong is with the Department of Mechanical and Energy Engineering, Southern University of Science and Technology, Shenzhen 518055, China (e-mail: he.kong@uon.edu.au).

Digital Object Identifier 10.1109/LRA.2022.3194684

work. Support lemmas and closely related definitions are given in the Appendix.

II. Geometry of Some Matrix Groups for Robotics

In this section, we review Lie groups for robotics [17, Cha. 7]. The motion of a rigid body with respect to (w.r.t.) a reference frame can be described by an element of the special Euclidean group denoted as $SE(3)$. It consists of a rotation matrix in the special orthogonal group $\mathbf{R} \in SO(3)$, and a translation vector $\mathbf{t} \in \mathbb{R}^3$ as follows: $\begin{pmatrix} \mathbf{R} & t \\ 0 & 1 \end{pmatrix}$. The Lie algebra of $SE(3)$ is denoted by $\mathfrak{se}(3)$, and an element of it has the form $\begin{pmatrix} \omega^\wedge & \mathbf{v} \\ \mathbf{0} & 0 \end{pmatrix}$, where $\omega^\wedge$ is the matrix representation of a vector $\omega \in \mathbb{R}^3$ using the "hat" operator[1]: $\omega^\wedge = \begin{pmatrix} 0 & -\omega_3 & \omega_2 \\ \omega_3 & 0 & -\omega_1 \\ -\omega_2 & \omega_1 & 0 \end{pmatrix} \in \mathfrak{so}(3)$. For simplicity, we express $SE(3)$ compactly as $(\omega, \mathbf{v})$.

The matrix Lie group $SE_n(3)$, first introduced in [18] and [19], is known as the group of n direct isometries, which is comprised of a rotation matrix in $\mathbf{R} \in SO(3)$ and n vectors $t_i \in \mathbb{R}^3$ and is usually used in the simultaneous localization and mapping (SLAM) to represent states including features. The matrix representations of an element in $SE_n(3)$ and an element in its Lie algebra $\mathfrak{se}_n(3)$ are:

$$\left(\begin{array}{c|ccc} \mathbf{R} & \mathbf{t}_1 & \cdots & \mathbf{t}_n \\ \hline \mathbf{0} & & \mathbf{I} & \end{array}\right), \quad \left(\begin{array}{c|ccc} \omega^\wedge & \mathbf{v}_1 & \cdots & \mathbf{v}_n \\ \hline \mathbf{0} & & \mathbf{0} & \end{array}\right).$$

The adjoint action of $\mathbf{X} \in SE_n(3)$ on $\mathbf{y} \in \mathfrak{se}_n(3)$ is defined as $\mathrm{Ad}_{\mathbf{X}} : \mathfrak{se}_n(3) \to \mathfrak{se}_n(3), \mathbf{y} \mapsto \mathbf{X}\mathbf{y}\mathbf{X}^{-1}$. The differential of the adjoint action $\mathrm{Ad}_{\mathbf{X}}$ at the identity element of $SE_n(3)$, denoted as $\mathrm{ad}_{\mathbf{x}} : \mathfrak{se}_n(3) \to \mathfrak{se}_n(3)$, is a linear mapping from $\mathfrak{se}_n(3)$ to itself. The matrix representations of the adjoint action of $SE_n(3)$ on $\mathfrak{se}_n(3)$ and the adjoint action of $\mathfrak{se}_n(3)$ on itself are:

$$\begin{pmatrix} \mathbf{R} & \mathbf{0} & \mathbf{0} & \mathbf{0} \\ \mathbf{t}_1^\wedge \mathbf{R} & \mathbf{R} & \mathbf{0} & \mathbf{0} \\ \vdots & \mathbf{0} & \ddots & \mathbf{0} \\ \mathbf{t}_n^\wedge \mathbf{R} & \mathbf{0} & \mathbf{0} & \mathbf{R} \end{pmatrix}, \quad \begin{pmatrix} \omega^\wedge & \mathbf{0} & \mathbf{0} & \mathbf{0} \\ \mathbf{v}_1^\wedge & \omega^\wedge & \mathbf{0} & \mathbf{0} \\ \vdots & \mathbf{0} & \ddots & \mathbf{0} \\ \mathbf{v}_n^\wedge & \mathbf{0} & \mathbf{0} & \omega^\wedge \end{pmatrix}. \tag{1}$$

The group $SE_2(3)$ originated from [12], shares the common structure of $SE_n(3)$, which usually represents states including an orientation $\mathbf{R}$, position $\mathbf{p}$ and velocity $\mathbf{v}$ of a rigid body:

$$SE_2(3) := \left\{ \left(\begin{array}{c|cc} \mathbf{R} & \mathbf{v} & \mathbf{p} \\ \hline \mathbf{0}_{2\times 3} & & \mathbf{I}_2 \end{array}\right) \middle| \mathbf{R} \in SO(3), \mathbf{p}, \mathbf{v} \in \mathbb{R}^3 \right\}.$$

The group and the Lie algebra are linked via the exponential and logarithm operations. To be specific, the exponential map of a matrix, $\exp : \mathfrak{se}_n(3) \to SE_n(3)$, allows us to wrap a Lie algebra element around the group. The exponential map is locally invertible at the neighborhood of the identity of the Lie group, in which it is injective. We then can define the logarithm mapping $\log : SE_n(3) \to \mathfrak{se}_n(3)$ as the inverse of the exponential mapping within the neighborhood.

III. Logarithmic Invariant Error Propagation

In this section, we present the closed-form error dynamics on $\mathfrak{se}_n(3)$ without any approximation and elucidate that the nonlinearity of error propagation dynamics is caused by the introduction of the noise to the system.

A. Uncertainty Propagation in Dynamics

Consider the following system on a matrix group $SE_n(3)$:

$$\dot{\mathbf{X}} = \mathbf{X}\mathbf{v}_b + \mathbf{v}_g\mathbf{X} + f_0(\mathbf{X}), \text{with} \mathbf{X}(0) = \mathbf{X}_0, \tag{2}$$

where $\mathbf{X} \in SE_n(3)$ is the system state, $\mathbf{v}_b, \mathbf{v}_g \in \mathfrak{se}_n(3)$ are inputs, and f_0 is a vector filed, a smooth mapping from $SE_n(3)$ to its tangent bundle $T(SE_n(3))$. In practice, $\mathbf{X}$ represents the configuration of a robot action space, $\mathbf{v}_b$ represents the input in the body frame, and $\mathbf{v}_g$ represents the input in the fixed frame.

We consider another dynamical system governed by the same vector field f_0, but differently initialized and steered by a noisy input $\mathbf{v}_b^{(n)}$, that is,

$$\dot{\bar{\mathbf{X}}} = \bar{\mathbf{X}}\mathbf{v}_b^{(n)} + \mathbf{v}_g\bar{\mathbf{X}} + f_0(\bar{\mathbf{X}}), \text{with} \bar{\mathbf{X}}(0) = \bar{\mathbf{X}}_0, \tag{3}$$

$\mathbf{v}_b^{(n)} = \mathbf{v}_b + \mathbf{w}$ where $\mathbf{w}^\vee \in \mathbb{R}^{3(n+1)}$ is assumed to be a noise[2]. The trajectory $\bar{\mathbf{X}}$ performs an open-loop tracking of $\mathbf{X}$. The input $\mathbf{v}_b^{(n)}$ is from body-fixed motion sensors, such as accelerates and perimeters, and $\mathbf{w}$ then captures the sensor noise.

Following [12], we introduce two forms of errors between trajectories $\mathbf{X}$ and $\bar{\mathbf{X}}$ in the sense of group multiplication, which can be viewed as the group analog of linear errors in a vector space.

Definition 1 (Invariant Errors): The left (right) invariant error of the trajectories $\mathbf{X}$ and $\hat{\mathbf{X}}$ is defined respectively as follows:

$$\eta_L := \mathbf{X}(t)^{-1}\bar{\mathbf{X}}(t) \quad \text{(left invariant error)}, \tag{4}$$

$$\eta_R := \bar{\mathbf{X}}(t)\mathbf{X}(t)^{-1} \quad \text{(right invariant error)}. \tag{5}$$

The letter [12] studies a class of group affine dynamics generalizing linear systems, which are of the form

$$\dot{\mathbf{X}} = f_u(\mathbf{X}),$$

where $f_u : SE_n(3) \to T(SE_n(3))$ satisfies the so-called group affine property for any $u \in \mathcal{U}, \mathbf{X}_1, \mathbf{X}_2 \in SE_n(3)$,

$$f_u(\mathbf{X}_1\mathbf{X}_2) = \mathbf{X}_1 f_u(\mathbf{X}_2) + f_u(\mathbf{X}_1)\mathbf{X}_2 - \mathbf{X}_1 f_u(I)\mathbf{X}_2. \tag{6}$$

Different from (6), in this letter we require that $f_0(\cdot)$ satisfies

$$f_0(\mathbf{X}_1\mathbf{X}_2) = f_0(\mathbf{X}_1)\mathbf{X}_2 + \mathbf{X}_1 f_0(\mathbf{X}_2). \tag{7}$$

One can verify that with $f_0(\cdot)$ satisfying (7), the dynamics of the invariant errors becomes:

$$\dot{\eta}_L = -\mathbf{v}_b\eta_L + \eta_L\mathbf{v}_b + \eta_L\mathbf{w} + f_0(\eta_L), \text{(left invariant)} \tag{8}$$

$$\dot{\eta}_R = \mathbf{v}_g\eta_R - \eta_R\mathbf{v}_g + \mathrm{Ad}_{\bar{\mathbf{X}}}\mathbf{w}\eta_R + f_0(\eta_R), \text{(right invariant)}. \tag{9}$$

Note that the dynamics of (2) satisfies the group affine property (6) and the left-invariant dynamics (8) and the right-invariant dynamics (9) satisfy (7).

Since the Lie algebra can be thought of as infinitesimal motions near the identity of a Lie group, we define an error vector $\xi \in \mathbb{R}^{3(n+1)}$ called the logarithmic invariant error as follows:

$$\xi = \log(\eta)^\vee. \tag{10}$$

[1]If not specifically in the $SO(3)$ group, the "hat" operation $(\cdot)^\wedge$ will denote a linear mapping that the Lie algebra $\mathfrak{g}$ can be identified into $\mathbb{R}^{\dim(\mathfrak{g})}$.

[2]The operation $(\cdot)^\vee$, called "vee" operation, is the inverse of the "hat" operation, which is a mapping from $\mathfrak{se}_n(3)$ to $\mathbb{R}^{3(n+1)}$.

For ease of notations, for an error $\eta \in SE_n(3)$, let $\xi := \begin{pmatrix}\omega & \mathbf{v}_1 & \cdots & \mathbf{v}_n\end{pmatrix}^\top$ denote the corresponding Lie logarithm of it, where $\omega^\wedge \in \mathfrak{so}_3$ and $\mathbf{v}_i \in \mathbb{R}^3$. In what follows, we give our main results on the dynamical evolution of ξ for both the left and the right invariant errors.

Theorem 1: Consider the dynamics (8), (9) of η where f_0 satisfies (7). The dynamics of ξ in (10) is given by:

Left invariant

$$\dot{\xi}_L = -\mathrm{ad}_{\mathbf{v}_b}\xi_L + \mathbf{J}(-\mathrm{ad}_{\xi_L^\wedge})^{-1}\mathbf{w}^\vee + \mathbf{A}\xi_L, \tag{11}$$

Right invariant

$$\dot{\xi}_R = \mathrm{ad}_{\mathbf{v}_g}\xi_R + \mathbf{J}(\mathrm{ad}_{\xi_R^\wedge})^{-1}\mathrm{Ad}_{\hat{\mathbf{X}}}\mathbf{w}^\vee + \mathbf{A}\xi_R, \tag{12}$$

where $\mathbf{A} = \frac{\partial}{\partial \xi} f_0(\exp(\xi))$ and $\mathbf{J}(\mathrm{ad}_{\mathbf{x}}) := \sum_{i=0}^{\infty} \frac{1}{(i+1)!}(\mathrm{ad}_{\mathbf{x}})^i$ which is defined in Definition 2 in the Appendix, called the left Jacobians of $\mathbf{x}$ for $\mathbf{x} \in \mathfrak{se}_n(3)$.

Proof: We only give proof for the left-invariant error case. For the right invariant case, it is similar and skipped.

Denote $\xi := \begin{pmatrix}\omega & \mathbf{v}_1 & \ldots & \mathbf{v}_n\end{pmatrix}$. By (1), the matrix $\mathrm{ad}_{\xi^\wedge}$ has eigenvalues up to multiplicity as follows:

$$\lambda_1 = 0 \quad \lambda_2 = |\omega|\,\mathbf{i} \quad \lambda_3 = -|\omega|\,\mathbf{i}.$$

From Theorem 5 of [20], i.e., the derivative of exponential, together with (8), we obtain that

$$\eta(t)^{-1}\dot{\eta}(t) = \sum_{i=0}^{\infty} \frac{(-1)^i}{(i+1)!}(\mathrm{ad}_{\xi^\wedge})^i \dot{\xi}^\wedge$$

$$\text{i.e.,} \quad \mathbf{v}_b - \exp(-\xi^\wedge)\mathbf{v}_b \exp(\xi^\wedge)$$

$$+ \mathbf{w} + \exp(-\xi^\wedge) f_0(\exp(\xi^\wedge)) = \sum_{i=0}^{\infty} \frac{(-1)^i}{(i+1)!}(\mathrm{ad}_{\xi^\wedge})^i \dot{\xi}.$$

By Lemma 1 and adjoint representation of a Lie algebra, the above equation becomes $(\mathbf{I} - \mathrm{e}^{-\mathrm{ad}_{\xi^\wedge}})\mathbf{v}_b^\vee + \mathbf{w}^\vee + (\exp(-\xi^\wedge) f_0(\exp(\xi^\wedge)))^\vee = \frac{\mathbf{I} - e^{-\mathrm{ad}_{\xi^\wedge}}}{\mathrm{ad}_{\xi^\wedge}}\dot{\xi}$. Note that when ω satisfies $|\omega| \neq 2k\pi$ $(k = 1, 2, \ldots)$, $\frac{\mathbf{I} - e^{-\mathrm{ad}_{\xi^\wedge}}}{\mathrm{ad}_{\xi^\wedge}}$ is invertible. Since the logarithm is defined within the injectivity radius around the identity of $\mathfrak{se}_n(3)$, we have $|\omega| \neq 2k\pi, k = 1, 2, \ldots$ which together with the above equation yields that

$$\dot{\xi} = \mathrm{ad}_{\xi^\wedge}\mathbf{v}_b^\vee + \left(\frac{\mathbf{I} - e^{-\mathrm{ad}_{\xi^\wedge}}}{\mathrm{ad}_{\xi^\wedge}}\right)^{-1}\mathbf{w}^\vee + g_0(\xi) \tag{13}$$

where $g_0(\xi) := (\eta(t)\frac{\mathbf{I} - e^{-\mathrm{ad}_{\xi(t)}}}{\mathrm{ad}_{\xi(t)}})^{-1} f_0(\exp(\eta))$. Now we will show that the mapping $g_0(\cdot) : x \mapsto \mathbf{A}x$ is a linear mapping. Consider a state $\eta^\star \in SE_n(3)$ which satisfies $\dot{\eta^\star} = f_0(\eta^\star)$ and a vector of its logarithm denoted as $\xi^\star$. By Theorem 7 of [12] and the property of f_0 (7), the vector $\xi^\star$ have the following dynamic

$$\dot{\xi}^\star = \mathbf{A}\xi^\star.$$

From Theorem 5 of [20], i.e., the derivative of exponential, the vector $\xi^\star$ writes

$$\dot{\xi}^\star = g_0(\xi^\star).$$

Therefore, we conclude that $g_0(\xi^\star) = \mathbf{A}\xi^\star$. Finally, (13) can be written as

$$\begin{aligned}\dot{\xi}(t) &= \mathrm{ad}_{\xi^\wedge}\mathbf{v}_b^\vee + \left(\frac{\mathbf{I} - e^{-\mathrm{ad}_{\xi^\wedge}}}{\mathrm{ad}_{\xi^\wedge}}\right)^{-1}\mathbf{w}^\vee + g_0(\xi) \\ &= -\mathrm{ad}_{\mathbf{v}_b}\xi + \mathbf{J}(-\mathrm{ad}_{\xi^\wedge})^{-1}\mathbf{w}^\vee + \mathbf{A}\xi,\end{aligned}$$

which completes the proof. □

The closed-form evolution of noisy $\xi(t)$ is provided by Theorem 1, which is described by a stochastic differential equation (SDE) in $\mathbb{R}^{3(n+1)}$. Though it is only the noisy terms in (11) and (12) that cause the noisy dynamics to be nonlinear, Gaussianity of the distribution of $\xi(t)$ is not closed under the propagation given by (11) and (12). Finding a solution to the SDE is involved, and will be investigated in our future work.

Remark 1 (Relations with Existing Works): In the existing literature [12], the dynamics of the logarithmic invariant error has been shown to satisfy a log-linear property when the dynamics (8) and (9) are noise free, while in the presence of noise $\mathbf{w}$, the noise term is tackled by linear approximation [12]. In this letter, we analyze the influence of the noise on the logarithmic invariant error propagation via the derivative of the matrix exponential. When the left Jacobians of the error are approximated to the identity by first-order linearization, our result boils down to results in [5], [12], [16], [21]. More about the linearization approximation in $SE_2(3)$ will be discussed in Section IV-B.

IV. Applications in VINS

We will customize the right invariant error result on the $SE_2(3)$ group to IMU and apply it to analyze the IMU kinematics. Based on these theoretical results, we further design a filtering algorithm for state estimation of a mobile robot with the IMU in the realtime vision-aided inertial navigation scenario.

A. Logarithmic Right Invariant Error Propagation on the $SE_2(3)$

We are interested in estimating a rigid body's 3D orientation, position, and velocity in the world frame, given angular velocity and acceleration measurements from the IMU attached to the rigid body. The above collection of variables forms the state variable of IMU and can be represented in the world frame as an element of $SE_2(3)$. To be specific, the IMU state $\mathbf{X}_I(t)$ at time t can be expressed as:

$$\mathbf{X}_I(t) = \left(\begin{array}{c|cc}\mathbf{R}(t) & \mathbf{p}(t) & \mathbf{v}(t) \\ \mathbf{0}_{2\times 3} & \multicolumn{2}{c}{\mathbf{I}_2}\end{array}\right)$$

where

i) $\mathbf{R}(t) \in SO(3)$ represents the rotation of the rigid body relative to the reference frame, reflecting the rotation from the world frame to the body frame attached to the rigid body;
ii) $\mathbf{p}(t) \in \mathbb{R}^3$ and $\mathbf{v}(t) \in \mathbb{R}^3$ are the position and velocity relative to the world frame, respectively.

The continuous-time kinematics of the orientation, velocity and position of the IMU are respectively described as follows:

$$\dot{\mathbf{R}}(t) = \mathbf{R}(t)\omega(t)^\wedge, \quad \dot{\mathbf{p}}(t) = \mathbf{v}(t), \quad \dot{\mathbf{v}}(t) = \mathbf{a}(t), \tag{14}$$

where $\boldsymbol{\omega}$ denotes the angular velocity relative to the body frame and $\mathbf{a}$ denotes the acceleration relative to the world frame.

Because the measurements of ω and $\mathbf{a}$ suffer from gyroscope and accelerometer bias, IMU measurements ω_m and $\mathbf{a}_m$ are usually modeled as the true angular velocity and linear acceleration variables corrupted by additive Gaussian white noise plus measurement biases:

$$\begin{aligned}\boldsymbol{\omega}_m(t) &= \boldsymbol{\omega}(t) + \mathbf{b}_\omega(t) + \mathbf{n}_\omega(t),\\ \mathbf{a}_m(t) &= \mathbf{R}(t)^{-1}\left(\mathbf{a}(t) - \mathbf{g}\right) + \mathbf{b}_a(t) + \mathbf{n}_a(t),\end{aligned} \tag{15}$$

where $\mathbf{g}$ denotes the gravitational acceleration relative to the world frame, and $\mathbf{n}_\omega$ and $\mathbf{n}_a$ are Gaussian noises, and $\mathbf{b}_\omega$ and $\mathbf{b}_a$ are the gyro and accelerometer biases. Typically, the biases are further modeled as stochastic processes driven by white Gaussian noises, that is,

$$\dot{\mathbf{b}}_\omega(t) = \mathbf{n}_{b_\omega}(t), \quad \dot{\mathbf{b}}_a(t) = \mathbf{n}_{b_a}(t).$$

Therefore, using the IMU measurements, the dynamics of the whole state $\mathbf{X}_I(t)$ can be given in a compact form:

$$\dot{\mathbf{X}}_I(t) = \mathbf{M}\mathbf{X}_I(t)\mathbf{N} + \mathbf{X}_I(t)\mathbf{v}_b(t) + \mathbf{v}_g(t)\mathbf{X}_I(t), \tag{16}$$

where $\mathbf{M} := \begin{pmatrix}\mathbf{I}_3 & \mathbf{0}_{3\times 2}\\ \mathbf{0}_{2\times 3} & \mathbf{0}_2\end{pmatrix}$ and $\mathbf{N} := \left(\begin{array}{c|cc}\mathbf{0}_{4\times 3} & \mathbf{0}_{4\times 2}\\ \hline \mathbf{0}_{1\times 3} & \begin{smallmatrix}1 & 0\end{smallmatrix}\end{array}\right)$, and $\mathbf{v}_b := \left(\begin{array}{c|c}(\boldsymbol{\omega}_m - \mathbf{b}_\omega - \mathbf{n}_\omega)^\wedge & \mathbf{0}_{3\times 1}\ \ \mathbf{a}_m - \mathbf{b}_a - \mathbf{n}_a\\ \hline \mathbf{0}_{2\times 3} & \mathbf{0}_{2\times 2}\end{array}\right) \in \mathfrak{se}_2(3)$ and $\mathbf{v}_g := \left(\begin{array}{c|c}\mathbf{0}_{3\times 3} & \mathbf{0}_{3\times 1}\ \ \mathbf{g}\\ \hline \mathbf{0}_{2\times 3} & \mathbf{0}_{2\times 2}\end{array}\right) \in \mathfrak{se}_2(3)$ are inputs relative to the body frame and the world frame respectively. In (16), $\mathbf{M}\mathbf{X}_I(t)\mathbf{N}$ reflects the "autonomous" part of the dynamics.

An estimate $\hat{\mathbf{X}}_I$ to $\mathbf{X}_I$ can be propagated by making an estimate to $\mathbf{v}_b$ from the IMU measurements:

$$\dot{\hat{\mathbf{X}}}_I(t) = \mathbf{M}\hat{\mathbf{X}}_I(t)\mathbf{N} + \hat{\mathbf{X}}_I(t)\hat{\mathbf{v}}_b + \mathbf{v}_g(t)\hat{\mathbf{X}}_I(t) \tag{17}$$

with $\hat{\mathbf{v}}_b := \left(\begin{array}{c|c}(\boldsymbol{\omega}_m - \hat{\mathbf{b}}_\omega)^\wedge & \mathbf{0}_{3\times 1}\ \ \mathbf{a}_m - \hat{\mathbf{b}}_a\\ \hline \mathbf{0}_{2\times 3} & \mathbf{0}_2\end{array}\right)$. Note that the estimated biases maintain unchanged during the estimate propagation since the IMU measurement does not support us to refine our estimate to the device's biases, i.e., $\dot{\hat{\mathbf{b}}}_\omega = \mathbf{0}$ and $\dot{\hat{\mathbf{b}}}_a = \mathbf{0}$ for the propagation. We define the estimation error of the gyro and accelerometer biases as $\tilde{\mathbf{b}}_\omega := \hat{\mathbf{b}}_\omega - \mathbf{b}_\omega$ and $\tilde{\mathbf{b}}_a := \hat{\mathbf{b}}_a - \mathbf{b}_a$. The right invariant errors in (4) denoted by $\eta_I := \hat{\mathbf{X}}_I\mathbf{X}_I^{-1}$ for the state of IMU have the explicitly form:

$$\eta_I = \left(\begin{array}{c|ccc}\tilde{\mathbf{R}}(t) & \hat{\mathbf{p}}(t) - \tilde{\mathbf{R}}(t)\mathbf{p}(t) & \hat{\mathbf{v}}(t) - \tilde{\mathbf{R}}(t)\mathbf{v}(t)\\ \hline \mathbf{0}_{2\times 3} & \multicolumn{2}{c}{\mathbf{I}_2}\end{array}\right).$$

We then have the following results for the dynamics of the logarithmic invariant error, $\xi_I := \log(\eta_I)^\vee$.

Theorem 2: Consider the dynamics (16) and (17). The dynamics of $\xi_I \in \mathbb{R}^9$ is given by:

$$\dot{\xi}_I = \mathbf{A}\xi_I + \mathbf{J}(\mathrm{ad}_{\xi_I{}^\wedge})^{-1}\mathbf{B}\begin{pmatrix}-\tilde{\mathbf{b}}_\omega + \mathbf{n}_\omega\\ -\tilde{\mathbf{b}}_a + \mathbf{n}_a\end{pmatrix}, \tag{18}$$

where $\mathbf{A} := \begin{pmatrix}\mathbf{0} & \mathbf{0} & \mathbf{0}\\ \mathbf{0} & \mathbf{0} & \mathbf{I}_3\\ \mathbf{g}^\wedge & \mathbf{0} & \mathbf{0}\end{pmatrix}$ and $\mathbf{B} := \begin{pmatrix}\hat{\mathbf{R}} & \mathbf{0}\\ \hat{\mathbf{p}}^\wedge\hat{\mathbf{R}} & \mathbf{0}\\ \hat{\mathbf{v}}^\wedge\hat{\mathbf{R}} & \hat{\mathbf{R}}\end{pmatrix}$.

Proof: The dynamics of right invariant error η_I can be computed as

$$\begin{aligned}\dot{\eta_I} &= \dot{\hat{\mathbf{X}}}_I\mathbf{X}_I^{-1} - \mathbf{X}_I^{-1}\hat{\mathbf{X}}_I\dot{\mathbf{X}}_I\mathbf{X}_I^{-1}\\ &= \mathbf{v}_g\eta_I - \eta_I\mathbf{v}_g + \mathbf{M}\eta_I\mathbf{N} + \mathrm{Ad}_{\hat{\mathbf{X}}_I}\mathbf{W}\eta_I\end{aligned}$$

where $\mathbf{W} := \begin{pmatrix}-\tilde{\mathbf{b}}_\omega^\wedge + \mathbf{n}_\omega^\wedge & \mathbf{0} & -\tilde{\mathbf{b}}_a + \mathbf{n}_a\\ \mathbf{0} & \mathbf{0} & \mathbf{0}\end{pmatrix}$. By Theorem 1, we get (18), which completes the proof. □

B. Approximation Methods for Error Propagation

The error propagation in the Lie algebra is essentially a diffusion process driven by a white random process $\mathbf{w}(t)$ described by (18). The solution of the SDE depends on $\mathbf{J}(\mathrm{ad}_{\xi_I{}^\wedge})^{-1}\mathrm{Ad}_{\hat{\mathbf{X}}_I}$, causing mathematical difficulty in analysis. For estimation purposes, we will discuss on the following different approximations for the uncertainty propagation in an IMU.

1) *Under Small Invariant Error:* It is usually assumed that the error η_I is small enough, that is, η_I is sufficiently close to the identity as $\mathbf{X}_I$ tracks $\hat{\mathbf{X}}_I$ well so that the following approximation is viable: $\xi_I \approx 0$ and $\mathbf{J}(\mathrm{ad}_{\xi_I{}^\wedge})^{-1} \approx \mathbf{I}$. As a consequence, (18) can be significantly simplified. Now we define an augmented state for the IMU device as: $\begin{pmatrix}\mathbf{X}_I\\ \mathbf{b}\end{pmatrix}$, with $\mathbf{b} := \begin{pmatrix}\mathbf{b}_\omega\\ \mathbf{b}_a\end{pmatrix}$. Then the augmented error can be approximated in a compact form via adding the simple vector differences $\tilde{\mathbf{b}}$:[3]

$$\begin{pmatrix}\dot{\xi}_I\\ \dot{\tilde{\mathbf{b}}}\end{pmatrix} \approx \begin{pmatrix}\mathbf{A} & -\mathbf{B}\\ \mathbf{0} & \mathbf{0}\end{pmatrix}\begin{pmatrix}\xi_I\\ \tilde{\mathbf{b}}\end{pmatrix} + \begin{pmatrix}\mathbf{B} & \mathbf{0}\\ \mathbf{0} & \mathbf{I}_2\end{pmatrix}\mathbf{n}_{\mathrm{imu}} \tag{19}$$

where $\mathbf{n}_{\mathrm{imu}} := (\mathbf{n}_\omega^\top\mathbf{n}_a^\top\mathbf{n}_{b_\omega}^\top\mathbf{n}_{b_a}^\top)^\top$ denotes the total IMU internal device noise, which are assumed to follow a normal distribution $\mathcal{N}(0, \mathbf{Q}_{\mathrm{imu}})$. Note that the covariance $\mathbf{Q}_{\mathrm{imu}}$ of $\mathbf{n}_{\mathrm{imu}}$ is usually accessible through sensor calibration. When the bias error handling the bias and measurement noise denoted as $\tilde{\mathbf{b}}_i - \mathbf{n}_i$ in (18) for $i \in \{\omega, a\}$ is sufficiently small, the closed-form formula can also be approximated as (19). The propagation result is essentially the same with the uncertainty propagation proposed in [5] and [16]. We derive the result from a different formula, and it clarifies how the bias error affects the uncertainty propagation.

2) *Imitating Jacobians of Invariant Error to Compensate Error Covariance Propagation:* Approximation as we do in (i) for (19) leads to inaccurate covariance propagation when ξ_I is large. To tackle this problem, we propose to use an additional variable, termed ξ_δ, drawn independently from some certain distribution to replace ξ_I in $\mathbf{J}(\mathrm{ad}_{\xi^\wedge})$. By doing so, we have a new approximation of (18) as follows:

$$\begin{pmatrix}\dot{\xi}_I\\ \dot{\tilde{\mathbf{b}}}\end{pmatrix} \approx \underbrace{\begin{pmatrix}\mathbf{A} & -\mathbf{J}_\delta^{-1}\mathbf{B}\\ \mathbf{0} & \mathbf{0}\end{pmatrix}}_{\mathbf{F}}\begin{pmatrix}\xi_I\\ \tilde{\mathbf{b}}\end{pmatrix} + \underbrace{\begin{pmatrix}\mathbf{J}_\delta^{-1}\mathbf{B} & \mathbf{0}\\ \mathbf{0} & \mathbf{I}_2\end{pmatrix}}_{\mathbf{G}}\mathbf{n}_{\mathrm{imu}}. \tag{20}$$

The above approximation is unrealistic in the sense that we cannot construct an estimate $\mathbf{X}_I$ in any way in practice to generate such ξ_I evolving like the right-hand side of (20). However, we can work out a better estimation error covariance using (20). Let $\mathbf{P}(t) := \mathbb{E}[(\xi_I\tilde{\mathbf{b}})(\xi_I\tilde{\mathbf{b}})^\top]$ denote the estimate error covariance. In virtue of (20), we use the following equation to approximate the evolution

[3]The augmentation technique is also used for developing "imperfect" IEKF in [19]. The introduction of additional vector difference coins the term of "imperfect" IEKF, since it sacrifices all the properties of the IEKF, see [19] for details.

of $\mathbf{P}(t)$:

$$\dot{\mathbf{P}} = \mathbf{F}\mathbf{P} + \mathbf{P}\mathbf{F}^\top + \mathbf{G}\mathbf{Q}_{\text{imu}}\mathbf{G}^\top \tag{21}$$

with $\mathbf{F}$ and $\mathbf{G}$ given in (20).[4] Compared to the exact and complex error covariance propagation, numerical integration under (21) is more viable in terms of computation efficiency to predict the error covariance to the next measurement sampling time since ξ_δ can be independently drawn beforehand. Note that the estimation error is seldom zero most of the time and sometime may be large due to external disturbance in the experiment. Hence the "trick" that uses $\mathbf{F}$ and $\mathbf{G}$ in (20) to propagate the covariance works better than the linearization approximation technique in most cases. Regarding the problem of choosing a good distribution for ξ_δ, our experimental experience is reported in Section V-A. Our current understanding of this issue is far from sufficient, and we may need further investigation on it in future work.

C. Logarithmic Invariant Error Propagation in VINS

In this part, we apply the theoretical results to filter design for motion state estimation of a mobile robot with the IMU in a real-time VINS application. Now suppose there are n landmarks, the positions of which denoted as $\mathbf{f} = (\mathbf{f}_1 \cdots \mathbf{f}_n)$. In VINS, we need to estimate the robot's real-time attitude and position as well as the positions of the landmarks. The system state, including the robot's pose and the landmarks' position, should be augmented to an element in $SE_{n+2}(3)$, that is,

$$\left(\begin{array}{c|ccc} \mathbf{R} & \mathbf{p} & \mathbf{v} & \mathbf{f} \\ \hline \mathbf{0}_{3\times 3} & \multicolumn{3}{c}{\mathbf{I}_3} \end{array}\right)$$

and the right invariant error for an estimate can be expressed as

$$\left(\begin{array}{c|ccc} \tilde{\mathbf{R}} & \hat{\mathbf{p}} - \tilde{\mathbf{R}}\mathbf{p} & \hat{\mathbf{v}} - \tilde{\mathbf{R}}\mathbf{v} & \hat{\mathbf{f}} - \tilde{\mathbf{R}}\mathbf{f} \\ \hline \mathbf{0}_{3\times 3} & \multicolumn{3}{c}{\mathbf{I}_3} \end{array}\right).$$

In this letter we consider spatially static landmarks with $\dot{\mathbf{f}} = 0$. Let ξ_X denote the logarithm invariant error. Since the system dynamics satisfies the form of (2), by Theorem 1, we obtain

$$\begin{pmatrix} \dot{\xi}_X \\ \dot{\tilde{\mathbf{b}}} \end{pmatrix} = \underbrace{\begin{pmatrix} \mathbf{A}_f & -\mathbf{B}_f \\ \mathbf{0} & \mathbf{0} \end{pmatrix}}_{\mathbf{F}} \underbrace{\begin{pmatrix} \xi_X \\ \tilde{\mathbf{b}} \end{pmatrix}}_{\mathbf{e}} + \underbrace{\begin{pmatrix} \mathbf{B}_f & \mathbf{0} \\ \mathbf{0} & \mathbf{I}_2 \end{pmatrix}}_{\mathbf{G}} \mathbf{n}_{\text{imu}}$$

$$\mathbf{A}_f = \begin{pmatrix} \mathbf{0} & \mathbf{0} & \mathbf{0} & \mathbf{0} \\ \mathbf{0} & \mathbf{0} & \mathbf{I}_3 & \mathbf{0} \\ \mathbf{g}^\wedge & \mathbf{0} & \mathbf{0} & \mathbf{0} \\ \mathbf{0} & \mathbf{0} & \mathbf{0} & \mathbf{0} \end{pmatrix} \quad \mathbf{B}_f = \mathbf{J}(\text{ad}_{\xi_X{}^\wedge})^{-1} \begin{pmatrix} \hat{\mathbf{R}} & \mathbf{0} \\ \hat{\mathbf{p}}^\wedge\hat{\mathbf{R}} & \mathbf{0} \\ \hat{\mathbf{v}}^\wedge\hat{\mathbf{R}} & \hat{\mathbf{R}} \\ \hat{\mathbf{f}}^\wedge\hat{\mathbf{R}} & \mathbf{0} \end{pmatrix}. \tag{22}$$

The approximation methods provided in Section IV-B can also be applied to approximate $\mathbf{B}_f$.

[4]The solution to this matrix differential equation (21) is computed by $\mathbf{P}_{t_{k+1}} = \Phi(t_{k+1}, t_k)\mathbf{P}_{t_k}\Phi(t_{k+1}, t_k)^\top + \mathbf{Q}_d$ where $\Phi(t_{k+1}, t_k) = \exp(\mathbf{F}\delta t)$ is the state transition matrix and $\mathbf{Q}_d \approx \Phi(t_{k+1}, t_k)\mathbf{P}_{t_k}\Phi(t_{k+1}, t_k)^\top \delta t$ is the approxiamated discrete noise covariance [22].

D. Visual Measurements Update in VINS

In the VINS problem, external feature positions measurements should be obtained by the camera. The camera's pose relative to the world frame can be expressed in terms of the IMU's pose and position as well as the relative pose and position between the camera and IMU:

$$\mathbf{X}_C = \begin{pmatrix} \mathbf{R} & \mathbf{p} \\ 0 & 1 \end{pmatrix} \mathbf{X}_I^C,$$

where $\mathbf{X}_I^C := \begin{pmatrix} \mathbf{R}_I^C & \mathbf{p}_I^C \\ 0 & 1 \end{pmatrix} \in SE(3)$ encodes the relative rotation $\mathbf{R}_I^C$ from the IMU frame to the camera one as well as the relative position $\mathbf{p}_I^C$ of the origin of the camera frame relative to the IMU frame. In practice, $\mathbf{R}_I^C$ and $\mathbf{p}_I^C$ may be accurately obtained through hardware calibration.

When the camera is exploring the environment and tracking the landmark, the measurement model in the discrete-time form at time step k (the continuous-time form denoted as t_k) is defined as follows:

$$\mathbf{z}(k) = \boldsymbol{\pi}\left(\mathbf{X}_C(k)^{-1}\mathbf{f}\right) + \mathbf{n}_C(k) \quad \mathbf{n}_C \sim \mathcal{N}(0, \mathbf{N}) \tag{23}$$

where $\pi(\mathbf{x}) := \mathbf{K}\frac{\mathbf{x}}{\|\mathbf{x}\|}$ denotes the camera projection mapping with $\mathbf{K}$ being the camera intrinsic matrix, and $\mathbf{n}_C$ is the measurement noise. The linearized measurement equation w.r.t. the errors writes:

$$\tilde{\mathbf{z}} = \mathbf{z}(k+1) - \boldsymbol{\pi}\left(\hat{\mathbf{X}}_C(k+1|k)^{-1}\hat{\mathbf{f}}\right) = \mathbf{H}\mathbf{e} + O(\|\mathbf{e}\|^2)$$

$$\mathbf{H} = \partial\pi \cdot \mathbf{R}_I^{C-1}\hat{\mathbf{R}}^{-1}\begin{pmatrix} \mathbf{0}_3 & -\mathbf{I}_3 & \mathbf{0}_3 & \mathbf{0}_3 & \mathbf{0}_3 & \mathbf{I}_3 \end{pmatrix} \tag{24}$$

where $\partial\pi$ represents the projection Jacobian and $\hat{\mathbf{X}}_C(k+1|k)$ denotes *a priori* estimate state.

The IEKF update proceeds by calculating the Kalman gian:

$$\mathbf{K} = \mathbf{P}(k+1|k)\mathbf{H}^\top\left(\mathbf{H}\mathbf{P}(k+1|k)\mathbf{H}^\top + \mathbf{N}\right)^{-1}. \tag{25}$$

After obtaining the Kalman gain and the transformed residuals, the estimated state are corrected separately. Because of the right-invariant observation equation (23), the innovation also depends on the invariant error and the updated equation for the IMU pose $\mathbf{X}_I$ takes the following form [12]:

$$\hat{\mathbf{X}}_I(k+1|k+1) = \exp\left((\mathbf{K}\tilde{\mathbf{z}})_{[I]}\right)\hat{\mathbf{X}}_I(k+1|k), \tag{26}$$

where $(y)_{[x]}$ represents the row of the vector y corresponding with x. Because the bias cannot be added in the matrix group, their updated equation writes as follows

$$\hat{\mathbf{b}}(k+1|k+1) = \hat{\mathbf{b}}(k+1|k) + (\mathbf{K}\tilde{z})_{[\hat{\mathbf{b}}]}. \tag{27}$$

The corresponding covariance matrix is updated by:

$$\mathbf{P}(k+1|k+1) = (\mathbf{I} - \mathbf{K}\mathbf{H}_\mathbf{X})\,\mathbf{P}(k+1|k). \tag{28}$$

E. Discussion on the Estimators' Consistency

The observability of a dynamical system, which indicates whether we are capable of recovering the unknown parameters or the initial states of the system with a sequence of system output of a certain length, can be used for consistency analysis of an estimator design for the system [9], [23]. We will discuss the consistency of the proposed estimator via observability, following the work [9]. Note that irrespective of the estimate of $\mathbf{b}$ in (22), our logarithmic invariant error propagation is linear,

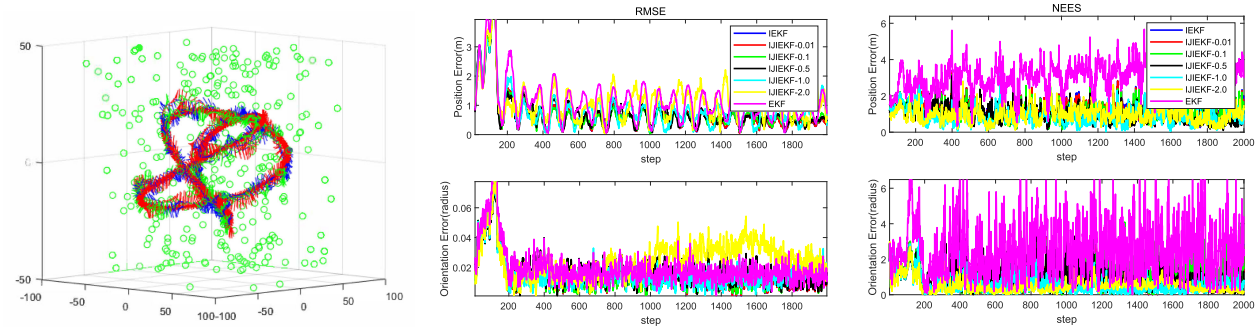

(a) Trajectory. (b) Root Mean Squared Error (RMSE). (c) Normalized Estimation Error Squared.

Fig. 1. The simulation results for 50 Monte-Carlo runs of **EKF**, **IEKF** and **IJ-IEKF** algorithms with $\xi_\delta \sim \mathcal{U}(-r, r)$, and we set $r = 0.01, 0.1, 0.5, 1.0, 2.0$. Fig. 1(a) shows the simulated trajectory with $[50\cos(0.075t), 40\sin(0.05t), 20\sin(0.05t+1)]^\top$. Fig. 1(b) and Fig. 1(c) show RMSE and NEES of the above-mentioned algorithms at every time step during experiments. (a) Trajectory (b) Root Mean Squared Error (RMSE) (c) Normalized Estimation Error Squared.

TABLE I
SIMULATIONS. ROOT MEAN SQUARED ERROR (RMSE) AND NORMALIZED ESTIMATION ERROR SQUARED (NEES)

	RMSE		NEES	
	Pos.(m)	**Ang.(rad)**	**Pos.**	**Ang.**
EKF	1.1520	0.0198	2.9966	2.5539
IEKF	0.6916	0.0147	1.1411	1.1221
IJIEKF-0.01	0.6871	**0.0146**	1.1218	1.1094
IJIEKF-0.1	**0.6839**	0.0150	1.0938	1.1389
IJIEKF-0.5	0.7548	0.0174	0.9815	1.0621
IJIEKF-1.0	0.8481	0.0161	0.9275	0.5528
IJIEKF-2.0	1.1619	0.0254	0.9871	0.5115

The bold entities represent the best performance of this statistics on RMSE performance.

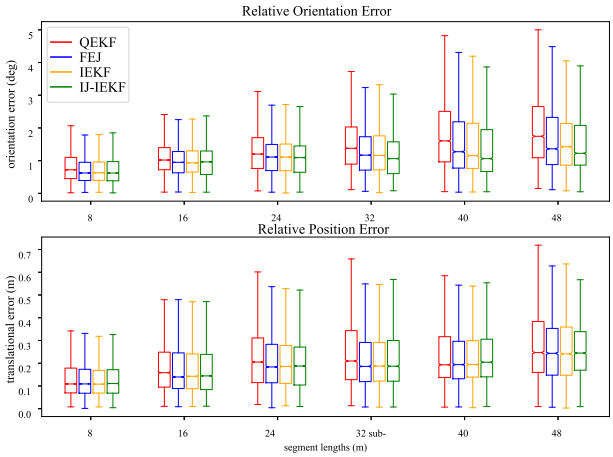

Fig. 2. Boxplots of the odometric relative pose error using **QEKF**, **FEJ**, **IEKF** and **IJ-IEKF** algorithms on different segments of easy, medium, and difficult sequences in the EuRoC MAV dataset.

TABLE II
EXPERIMENT PARAMETERS

Parameters	Value	Parameters	Value
Gyro White Noise$(\mathrm{rad}/(\mathrm{s}\sqrt{\mathrm{HZ}}))$	1.6968e-04	Gyro. Random Walk$(\mathrm{rad}/(\mathrm{s}^2\sqrt{\mathrm{HZ}}))$	1.9393e-05
Accel. White Noise$(\mathrm{m}/(\mathrm{s}^2\sqrt{\mathrm{HZ}}))$	2.0000e-3	Accel. Random Walk $(\mathrm{m}/(\mathrm{s}^3\sqrt{\mathrm{HZ}}))$	3.0000e-3
Max. Clone Size	11	Max Feats	40

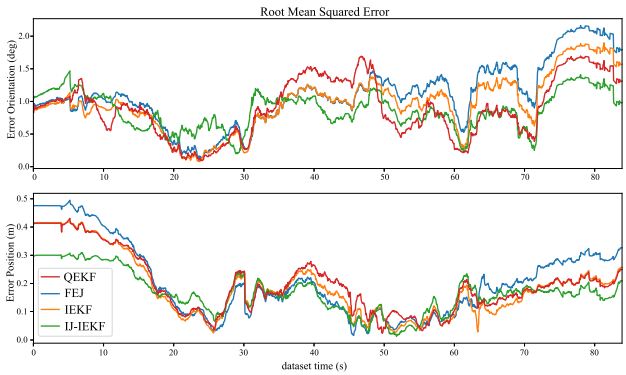

Fig. 3. The root mean squared errors evolution for the **QEKF**, **FEJ**, **IEKF** and **IJ-IEKF** algorithms on the challenging sequence **MH_04_difficult**.

time-invariant (To be precise, the linear dynamics is nilpotent.). In the discretized dynamical system for a given sampling period δt, the transition matrix is a matrix of polynomials in δt as follows:

$$\Phi = \exp\left(\mathbf{A}_f \delta t\right) = \begin{pmatrix} \mathbf{I} & \mathbf{0} & \mathbf{0} & \mathbf{0} \\ \frac{1}{2}\mathbf{g}^\wedge \delta t^2 & \mathbf{I} & \mathbf{I}\delta t & \mathbf{0} \\ \mathbf{g}^\wedge \delta t & \mathbf{0} & \mathbf{I} & \mathbf{0} \\ \mathbf{0} & \mathbf{0} & \mathbf{0} & \mathbf{I} \end{pmatrix}.$$

The observation matrix $\mathcal{O}$ is given by

$$\mathcal{O} = \begin{pmatrix} \mathbf{H} \\ \mathbf{H}\Phi \\ \mathbf{H}\Phi^2 \\ \vdots \end{pmatrix} = C \begin{pmatrix} \mathbf{0} & -\mathbf{I} & \mathbf{0} & \mathbf{I} \\ -\frac{1}{2}\mathbf{g}^\wedge \delta t^2 & -\mathbf{I} & -\mathbf{I}\delta t & \mathbf{I} \\ -2\mathbf{g}^\wedge \delta t^2 & -\mathbf{I} & -2\mathbf{I}\delta t^2 & \mathbf{I} \\ \vdots & \vdots & \vdots & \vdots \end{pmatrix}$$

where $C = \mathbf{I} \bigotimes \partial\pi \cdot \mathbf{R}_I^{C-1}\hat{\mathbf{R}}^{-1}$ and $\bigotimes$ denotes the kronecker product. The six columns of the matrix are linearly dependent, which is consistent with the nonlinear observability result of the original system [9]. Notice that the introduction of the imitative logarithmic invariant error ξ_δ in place of the non-accessible ξ_X in an estimator has nothing to do with the system observability. Hence, the linear approximation and the imitative invertible Jacobians design for the VINS maintain consistency.

TABLE III
EXPERIMENTS. ABSOLUTE TRAJECTORY ERROR(ATE)

$(^\circ)/(m)$	MH_01_easy	MH_02_easy	MH_03_medium	MH_04_difficult	MH_05_difficult	Average
QEKF	2.415 / 0.155	0.940 / **0.089**	1.737 / 0.109	1.003 / 0.222	1.228 / 0.266	1.465 / 0.168
FEJ	1.925 / 0.120	0.745 / 0.104	1.375 / **0.091**	1.201 / 0.245	**0.877** / 0.250	1.225 / 0.162
IEKF	1.930 / 0.120	0.763 / 0.098	1.281 / 0.096	1.062 / 0.215	0.916 / 0.250	1.191 / 0.156
IJ-IEKF	**1.890** / **0.113**	**0.723** / 0.108	**1.212** / 0.094	**0.909** / **0.183**	0.945 / **0.238**	**1.136** / **0.147**

The bold entities represent the best performance of this statistics in this dataset.

V. EXPERIMENTAL EVALUATION

We evaluate the proposed algorithm based on the closed-form expression of right invariant error propagation by simulations and experiments on datasets. We evaluate the consistency of our algorithms and standard extended Kalman filter by simulations. We compare the imitating Jacobians for Invariant Extended Kalman Filter (IJ-IEKF) with quaternion-based extended Kalman filter (QEKF) [24], first estimates Jacobian EKF (FEJ) [9], and IEKF in experiments.

A. Simulations

We leverage the open-source simulation in [16] to simulate VINS with the trajectory shown in Fig. 1(a) and implement 50 Monte-Carlo runs with the EKF, IEKF, and IJ-IEKF algorithms. For a fairer comparison with the existing results, the setup is similar to [16]. Different from this work, we use the IJ-IEKF method to show the impact of the left Jacobians with the uniform distributed random variables $\xi_\delta \sim \mathcal{U}(-r, r)$ where r denotes the range of invariant error and can be set heuristically from experimental experience. We then calculate $\mathbf{J}_\delta := \mathbf{J}(\mathrm{ad}_{\xi_\delta^\wedge})$ via Definition 2. Different ranges ($r = 0.01, 0.1, 0.5, 1.0, 2.0$) are set in the simulation to imitate the Jacobians of orientation errors. It is noted that the position errors to imitate are set as 0. The root mean squared error (RMSE) and the normalized estimation error squared (NEES), which has been divided by the degrees of freedoms of the state variables, are used for evaluation. Results are shown in Table I and Fig. 1.

As shown in Fig. 1(c), the IJ-IEKF and IEKF maintain consistency with different ranges r, while the EKF is not consistent. Table. I illustrates that imitating the invariant error to compensate the Jacobian term for covariance propagation process improves the filter performance compared with IEKF proposed in [16], which is also demonstrated in the following experiments. It is noted that the RMSE and NEES results are not consistent because the Jacobian term causes an inflation of the covariance in particular parameter settings.

B. Experiments on Datasets

We further evaluate the accuracy of our proposed algorithms by testing them on the EuRoC MAV Datasets [25], which are collected on board a macro aerial vehicle in indoor environments. All the experiments are implemented on the OPENVINS platform [6] with an Intel i7-11700 processor. We maintain the multi-state constraint Kalman filter (MSCKF) [26] frame in the OPENVINS for its efficiency, where online calibration and loop closure modules are turned off.

We run this experiment with QEKF, FEJ, IEKF, and our proposed IJ-IEKF. We set the imitating orientation satisfies $\mathcal{U}(-0.5, 0.5)$. The other experimental parameters settings are shown in Table II. We select all **MH room** sequences (including easy, medium, and difficult mode) in the EuRoC MAV Datasets to demonstrate the performance of the above-mentioned algorithms. We choose the relative pose error (RPE) and the absolute trajectory error (ATE) as evaluation metrics. In order to analyze the performance on a single dataset, we also choose the RMSE as another evaluation metric. The reader can refer to [27] to find more details on the evaluation metrics. In the whole experiment, it costs less than 10 ms to perform the propagation step and the update step in all filter-based algorithms with about 20 captured features each step.

The boxplots in Fig. 2 illustrate that the error distribution of IJ-IEKF is closer to 0 and more concentrated, especially in terms of relative orientation error. Moreover, we choose a representative challenging sequence **MH_04_difficult** to show the difference in performance among QEKF, FEJ, IEKF, and IJ-IEKF, as shown in Fig. 3. It illustrates that the odometry estimates from IJ-IEKF contain minimal drift to keep the estimated trajectory close to the ground truth most of the time during the experiment, especially on the orientation error at the end of the sequence. All the evaluations on the ATE metrics are summarized in Table III.

VI. CONCLUSIONS AND FUTURE WORK

In this letter, we demonstrated how the noisy nonlinear term influences the evolution of estimation error through theoretical analysis and experimental tests. We analyzed the invariant error on $SE_n(3)$ and derived a closed-form expression for the propagation of the Lie logarithm of the invariant error on $\mathfrak{se}_n(3)$. We applied our theoretical findings to the navigation model of IMU, and then the IMU model was implemented in VINS. The experimental results showed that the filter based on compensating the nonlinear terms seems likely to perform better in certain parameter settings. However, it is worth further study the sampling techniques of IJ-IEKF, the choice of distribution of the imitating variable and the optimal filtering design on the closed-form expression.

APPENDIX
SUPPORTING LEMMAS AND RELATED DEFINITIONS

Lemma 1: Given any $\mathbf{A}, \mathbf{B} \in \mathfrak{g}$, it holds that $e^{\mathbf{A}}\mathbf{B}e^{-\mathbf{A}} = e^{\mathrm{ad}_{\mathbf{A}}}\mathbf{B}$.

Proof: See the full version of this article [28, Appendix] for details. □

Definition 2 (Jacobian of $SE_n(3)$): For any Lie algebra $\mathbf{x} \in \mathfrak{se}_n(3)$, the left Jocabians of $\mathbf{x}$ is defined as

$$\mathbf{J}(\mathrm{ad}_{\mathbf{x}}) = \sum_{i=0}^{\infty} \frac{1}{(i+1)!}(\mathrm{ad}_{\mathbf{x}})^i, \tag{29}$$

which is called the (left) Jacobian of $SE_n(3)$.[5]

[5]More details about the left and right Jocobians of $SO(3)$ and $SE(3)$ are provided in Section 7.1.5 of [17].

Note that using the paremetrization $\mathbf{T} = \exp(\xi^\wedge)$ and the pertubation $\mathbf{T}' = \exp((\xi + \delta\xi)^\wedge)$, the logarithm of the difference (relative to $\mathbf{T}$) can be approximated as $\log(\mathbf{T}'\mathbf{T}^{-1})^\vee \approx \mathbf{J}(\mathrm{ad}_{\xi^\wedge})\delta\xi$ given that $\delta\xi$ is sufficiently small. When an element of the Lie algebra $\mathfrak{se}_n(3)$ is parameterized as $\mathbf{x}^\vee := \begin{pmatrix}\boldsymbol{\theta}^\top & v_1^\top & \cdots & v_n^\top\end{pmatrix}^\top$ where $\theta^\wedge \in \mathfrak{so}(3)$ and $v_i \in \mathbb{R}^3$, the left Jacobian of $SE_n(3)$ writes $\mathbf{J}(_{\mathbf{x}}) = \begin{pmatrix} \mathbf{J}(\theta^\wedge) & \mathbf{0} & \cdots & \mathbf{0} \\ \mathbf{Q}_\theta(v_1) & \mathbf{J}(\theta^\wedge) & \cdots & \vdots \\ \vdots & \mathbf{0} & \ddots & \mathbf{0} \\ \mathbf{Q}_\theta(\mathbf{v}_n) & \mathbf{0} & \cdots & \mathbf{J}(\theta^\wedge) \end{pmatrix}$ where $\mathbf{J}(\theta^\wedge) = \sum_{i=0}^{\infty} \frac{1}{(i+1)!}(\theta^\wedge)^i = \frac{\sin|\theta|}{|\theta|}\mathbf{I} + (1 - \frac{\sin|\theta|}{|\theta|})\frac{\theta\theta^\top}{|\theta|^2} + \frac{1-\cos|\theta|}{|\theta|^2}\theta^\wedge$ and $\mathbf{Q}_\theta(v_i) = \sum_{n=0}^{\infty}\sum_{m=0}^{\infty}\frac{1}{(n+m+2)!}(\theta^\wedge)^n v_i^\wedge (\theta^\wedge)^m$.

REFERENCES

[1] S. Leutenegger, S. Lynen, M. Bosse, R. Siegwart, and P. Furgale, "Keyframe-based visual–inertial odometry using nonlinear optimization," *Int. J. Robot. Res.*, vol. 34, no. 3, pp. 314–334, 2015.

[2] C. Campos, R. Elvira, J. J. G. Rodríguez, J. M. M. Montiel, and J. D. Tardós, "ORB-SLAM3: An accurate open-source library for visual, visual-inertial, and multimap slam," *IEEE Trans. Robot.*, vol. 37, no. 6, pp. 1874–1890, Dec. 2021.

[3] J. Wakulicz, H. Kong, and S. Sukkarieh, "Active information acquisition under arbitrary unknown disturbances," in *Proc. IEEE Int. Conf. Robot. Automat.*, 2021, pp. 8429–8435.

[4] M. Bloesch, M. Burri, S. Omari, M. Hutter, and R. Siegwart, "Iterated extended Kalman filter based visual-inertial odometry using direct photometric feedback," *Int. J. Robot. Res.*, vol. 36, no. 10, pp. 1053–1072, 2017.

[5] R. Hartley, M. Ghaffari, R. M. Eustice, and J. W. Grizzle, "Contact-aided invariant extended Kalman filtering for robot state estimation," *Int. J. Robot. Res.*, vol. 39, no. 4, pp. 402–430, 2020.

[6] P. Geneva, K. Eckenhoff, W. Lee, Y. Yang, and G. Huang, "OpenVINS: A research platform for visual-inertial estimation," in *Proc. IEEE Int. Conf. Robot. Automat.*, 2020, pp. 4666–4672.

[7] A. J. Krener, "The convergence of the extended Kalman filter," in *Directions in Mathematical Systems Theory and Optimization*, vol. 286. Berlin, Germany: Springer, 2003, pp. 173–182.

[8] S. Huang and G. Dissanayake, "Convergence and consistency analysis for extended Kalman filter based SLAM," *IEEE Trans. Robot.*, vol. 23, no. 5, pp. 1036–1049, Oct. 2007.

[9] G. P. Huang, A. I. Mourikis, and S. I. Roumeliotis, "Analysis and improvement of the consistency of extended Kalman filter based SLAM," in *Proc. IEEE Int. Conf. Robot. Automat.*, 2008, pp. 473–479.

[10] S. Bonnabel, P. Martin, and P. Rouchon, "Symmetry-preserving observers," *IEEE Trans. Autom. Control*, vol. 53, no. 11, pp. 2514–2526, Dec. 2008.

[11] S. Bonnabel, "Left-invariant extended Kalman filter and attitude estimation," in *Proc. IEEE 46th Conf. Decis. Control*, 2007, pp. 1027–1032.

[12] A. Barrau and S. Bonnabel, "The invariant extended Kalman filter as a stable observer," *IEEE Trans. Autom. Control*, vol. 62, no. 4, pp. 1797–1812, Apr. 2017.

[13] A. Barrau and S. Bonnabel, "Stochastic observers on lie groups: A tutorial," in *Proc. IEEE Conf. Decis. Control*, 2018, pp. 1264–1269 .

[14] M. Brossard, A. Barrau, P. Chauchat, and S. Bonnabel, "Associating uncertainty to extended poses for on lie group IMU preintegration with rotating earth," *IEEE Trans. Robot.*, vol. 38, no. 2, pp. 998–1015, Apr. 2022.

[15] Y. Yang, C. Chen, W. Lee, and G. Huang, "Decoupled right invariant error states for consistent visual-inertial navigation," *IEEE Robot. Automat. Lett.*, vol. 7, no. 2, pp. 1627–1634, Apr. 2022.

[16] K. Wu, T. Zhang, D. Su, S. Huang, and G. Dissanayake, "An invariant-EKF VINS algorithm for improving consistency," in *Proc. IEEE/RSJ Int. Conf. Intell. Robots Syst.*, 2017, pp. 1578–1585 .

[17] T. D. Barfoot, *State Estimation for Robotics*. Cambridge, U.K.: Cambridge Univ. Press, 2017.

[18] A. Barrau and S. Bonnabel, "An EKF-SLAM algorithm with consistency properties," 2015, *arXiv:1510.06263*.

[19] A. Barrau, "Non-linear state error based extended Kalman filters with applications to navigation," Ph.D. dissertation, Mines Paristech, Paris, France, 2015.

[20] M. Hunacek, *Lie Groups: An Introduction Through Linear Groups*, vol. 92. Cambridge, MA, USA: The Mathematical Gazette, pp. 380–382, 2008.

[21] A. Barrau and S. Bonnabel, "Invariant Kalman filtering," *Annu. Rev. Control Robot. Auton. Syst.*, vol. 1, pp. 237–257, 2018.

[22] P. S. Maybeck, *Stochastic Models, Estimation and Control*, vol. 3. Cambridge, MA, USA: Academic Press, 2012.

[23] D. Su, H. Kong, S. Sukkarieh, and S. Huang, "Necessary and sufficient conditions for observability of SLAM-based TDOA sensor array calibration and source localization," *IEEE Trans. Robot.*, vol. 37, no. 5, pp. 1451–1468, Oct. 2021.

[24] N. Trawny and S. I. Roumeliotis, "Indirect Kalman Filter for 3D Attitude Estimation," Dept. Comp. Sci. Eng., Univ. Minnesota, Tech. Rep. 2005-002, 2005.

[25] M. Burri et al., "The EuRoC micro aerial vehicle datasets," *Int. J. Robot. Res.*, vol. 35, no. 10, pp. 1157–1163, 2016.

[26] A. I. Mourikis and S. I. Roumeliotis, "A multi-state constraint Kalman filter for vision-aided inertial navigation," in *Proc. IEEE Int. Conf. Robot. Automat.*, 2007, pp. 3565–3572.

[27] Z. Zhang and D. Scaramuzza, "A tutorial on quantitative trajectory evaluation for visual(-inertial) odometry," in *Proc. IEEE/RSJ Int. Conf. Intell. Robots Syst.*, pp. 7244–7251, 2018.

[28] X. Li, H. Jiang, X. Chen, H. Kong, and J. Wu, "Closed-form error propagation on the $SE_n(3)$ group for invariant extended Kalman filtering with applications to VINS," Jun. 2022, *arXiv:2206.09100*.